Thermoelectric performance of films in the bismuth-tellurium and antimony-tellurium systems

Luciana W. da Silva,[a] Massoud Kaviany,[b] and Ctirad Uher[c]
University of Michigan, Ann Arbor, Michigan 48109

Coevaporated bismuth-tellurium and antimony-tellurium films were fabricated under various deposition conditions (controlled evaporation rates of individual species, substrate temperature, and substrate material), and their thermoelectric (TE) properties (Seebeck coefficient, electrical resistivity, and carrier concentration) were measured in search of optimal TE performance. The tellurium atomic concentration was varied from 48% to 74%, the substrate temperature ranged from 130 to 300 °C, and glass, mica, magnesium oxide, and sapphire substrates were used. The chemical composition and crystal structure of the films were recorded (using microprobe and x-ray diffractometer, respectively), analyzed, and compared with available standard Bi_2Te_3 and Sb_2Te_3 single-crystal samples. High-performance TE films had tellurium atomic concentration around 60% and were deposited at a substrate temperature between 260 and 270 °C. © *2005 American Institute of Physics*. [DOI: 10.1063/1.1914948]

I. INTRODUCTION

Telluride compounds have been extensively studied in the past decades, due to their high thermoelectric (TE) figure of merit Z_e at room temperature. In bulk materials, a dimensionless figure of merit Z_eT of 0.75 in p-$BiSb_2Te_3$, at 300 K, was reported about 40 years ago.[1] Since then, there has been modest progress in increasing Z_eT near room temperature. The highest value reported appears to be 1.14 for the $p-(Bi_2Te_3)_{0.25}(Sb_2Te_3)_{0.72}(Sb_2Se_3)_{0.03}$ alloy.[2]

The TE properties of telluride films (0.7–20 μm thick) measured at room temperature, for various deposition methods, substrate temperatures, and substrate materials, are listed in Fig. 1. Zou *et al.*[3] deposited n-Bi_2Te_3 and p-Sb_2Te_3 films by coevaporation, at a substrate temperature T_{sub} of 260 and 230 °C, respectively, with Z_eT of approximately 0.3 (thermal conductivity of 1.5 W/m K is assumed). Lim *et al.*[4] used electroplating, and the n-Bi_2Te_3 films exhibited notably low performance, compared with that reported by others. The properties of the p-$Bi_{2-x}Sb_xTe_3$ films were not fully characterized due to the poor reproducibility. Böttner *et al.*[5,6] used cosputtering, followed by annealing, to improve the TE properties.

Several approaches have been proposed to enhance Z_eT in thin-film TE materials. Using quantum-confinement effects, which allows for the manipulation of the Seebeck coefficient α_S by enhancing the density of states near the Fermi energy, Z_eT ranging from 1.3 to 1.6, at 300 K, was reported for PbSeTe/PbTe quantum dot superlattice structures.[7,8] Venkatasubramanian *et al.*[2] show Z_eT of 2.4 for p-type nanostructured superlattices of Bi_2Te_3/Sb_2Te_3 at room temperature. These are phonon-blocking/electron-transmitting superlattices, which are produced by alternately depositing thin (1–4 nm) films of Bi_2Te_3 and Sb_2Te_3. For n-type Bi_2Te_3/$Bi_2Te_{2.83}Se_{0.17}$, Z_eT of 1.4 is found. Exploring thermionic emission at interfaces, Vashaee and Shakouri[9] have recently shown that metal-base superlattices with tall barriers can achieve Z_eT larger than 5, at room temperature. A key requirement is the nonconservation of lateral momentum, which allows a higher number of electrons to participate in the thermionic emission process.

The motivation for the present work is the application of Bi_2Te_3 and Sb_2Te_3 (in their simplest form) as the n- and p-type elements, respectively, of a column-type micro-TE cooler.[10] Using coevaporation of the elements, we deposited bismuth-tellurium (Bi–Te) and antimony-tellurium (Sb–Te) thin films at various T_{sub} and compositions, seeking films with optimum TE performance. Although it is known that T_{sub} above 200 °C is needed for films with high Z_eT (or high power factor α_S^2/ρ_e, as reported in Fig. 1), the performance of telluride compound films formed at lower temperatures is also investigated, since in the device fabrication, the current TE film patterning method limits T_{sub} to values below 170 °C.[11] The effect of substrate material and crystal structure on the TE properties is also explored. Platinum is used as the substrate for the TE films in the micro-TE cooler fabrication (current is injected through metal connectors composed of Cr/Au/Ti/Pt layers, where Pt interfaces with the TE elements),[11] and so, it is of particular interest here.

II. FILM FABRICATION

The Bi–Te and Sb–Te films were deposited by coevaporation. Each of the elements (Bi, Sb, and Te shots are 99.999% pure) of the desired compound (from the Bi–Te or Sb–Te systems) is placed in a 17-cc molybdenum boat, which is connected to an independent power supply (controlled manually). The flux from each source is monitored with separate quartz-crystal sensors. The substrates are placed at a distance of 46 cm above the sources, and rotate at

[a]Department of Mechanical Engineering; electronic mail: ldasilva@umich.edu
[b]Author to whom correspondence should be addressed; also at Department of Mechanical Engineering; electronic mail: kaviany@umich.edu
[c]Department of Physics; electronic mail: cuher@umich.edu

Reference	Zou et al. [3]		Lim et al. [4]		Böttner et al. [5, 6]	
Fabrication Method	Co-Evaporation		Electroplating		Co-Sputtering	
Substrate Material	Glass		Au		N/R	
TE Film Material	p-Sb$_2$Te$_3$	n-Bi$_2$Te$_3$	p-Bi$_{2-x}$Sb$_x$Te$_3$	n-Bi$_2$Te$_3$	p-(Bi,Sb)$_2$Te$_3$	n-Bi$_2$Te$_3$
Substrate Temperature, T_{sub} (°C)	230	260	N/A	N/A	N/R	N/R
Seebeck coefficient, α_S (µV/K)	171	-228	N/R	-60	227	-155
Electrical resistivity, ρ_e (µΩ-m)	10.4	13.0	N/R	10.0	23	21
Power factor, α_S^2/ρ_e (mW/K^2-m)	2.80	3.99	N/R	0.36	2.24	1.14
Film thickness, L_{te} (µm)	0.7	0.7	20	20	10-20	10-20

FIG. 1. Reported deposition methods and properties of the n- and p-type telluride films. (N/A: Not/Available; N/R: Not/Reported).

a controlled speed. A resistive heater (placed above the substrate) can maintain a constant substrate temperature of up to 300 °C, which is measured by a type-K thermocouple located at a distance of 5 mm from the substrate edge. The calibration of this thermocouple was established by comparing its temperature with a second thermocouple attached directly at the back surface of the substrate, which was stationary. An additional film thickness monitor is used to measure the overall thickness of the deposited compound.

The pressure during deposition varied from 1×10^{-6} to 4×10^{-6} torr. The Bi and Sb deposition rates varied from 1 ± 0.1 to 2.5 ± 0.1 Å/s, while the Te rate varied from 2.5 ± 0.5 to 4.5 ± 0.5 Å/s. All substrates were cleaned prior to the deposition with acetone and isopropanol, and dried with N$_2$.

III. FILM CHARACTERIZATION

A. Crystal structure and composition

The microstructure of the films (grain size and orientation) was examined using a high-resolution scanning electron microscope (SEM), which is combined with a focussed ion-beam workstation. The latter was used for *in situ* preparation and analysis of sample cross sections. In order to prevent the damage to the surface grains by the ion beam, a platinum patch (1 µm thick) was deposited on top of each TE film, prior to the sectioning.

The orientation of the crystals in the films was determined from x-ray diffraction (XRD) analyses. The patterns were obtained using a Scintag powder x-ray diffractometer.

The relative concentration of the elements was measured, with an accuracy of ±2%, by an electron microprobe analyzer, and averaged over ten distinct locations for each sample.

B. Thermoelectric properties

The Seebeck coefficient α_S was measured at room temperature, under vacuum. In each case, data were collected from two films deposited at the same time on identical substrates, which were mounted as shown in Fig. 2. One end of the film (10–20 mm long and 2–4 mm wide) was thermally connected to a heat sink and the other end to a heater. The temperatures of the hot and cold sides (T_h and T_c, respectively) were measured with fine copper-constantan thermo-

couples. The Cu leads of the thermocouples were also used to measure the potential difference, $\Delta\varphi$, across the film. The Seebeck coefficient was determined by

$$\alpha_S = \frac{\Delta\varphi}{T_h - T_c}, \tag{1}$$

and the results were corrected for the thermopower of the Cu leads.

The electrical resistivity ρ_e was obtained using the standard four-probe method, also at room temperature, under vacuum. It is given by

$$\rho_e = \frac{R_e A_t}{L}, \tag{2}$$

where L is the film length (distance between the fine copper wires used for $\Delta\varphi$ measurement when an electrical current J_e is applied), A_t ($=wL_{te}$, i.e., product between the width w and the thickness L_{te}) is the film cross-section area, and R_e($=\Delta\varphi/J_e$) is the electrical resistance. The film thickness, L_{te}, was obtained from four different locations on the sample, with an accuracy of ±5%, using a surface profiler.

Hall-effect measurements were performed in a cryostat equipped with a superconducting (5 T) magnet. A magnetic field B and current J_e were applied, and R_e (or $\Delta\varphi$) was measured. Data were taken in both magnetic-field directions to eliminate effects due to any probe misalignment. The Hall coefficient R_H is given by
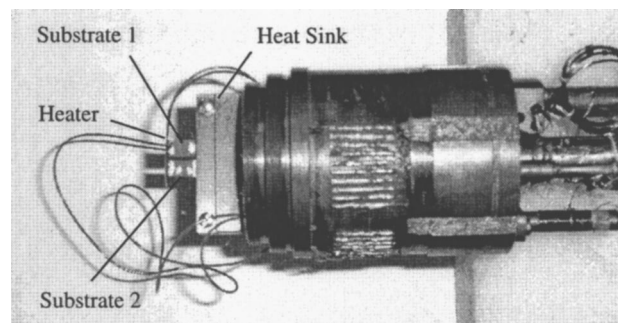

FIG. 2. Probe used for the Seebeck coefficient and electrical resistivity measurements. Two substrates, with the same TE film deposited on them, are held by the heat sink (cold side). The heater is attached to the opposite edge of the substrates (hot side). The electrical resistivity measurements are performed on substrate 2, while the Seebeck coefficient is obtained from both substrates.

TABLE I. Uncertainties of the measured and calculated properties.

Property	Uncertainty (%)
α_S	± 5
ρ_e	± 12
α_S^2/ρ_e	± 15
R_H	± 15
n_c	± 15
μ	± 20

$$R_H = R_e \frac{L_{te}}{B}, \tag{3}$$

and from that, the carrier concentration n_c and mobility μ were calculated using

$$n_c = \frac{1}{R_H e_c} \quad \text{and} \quad \mu = \frac{R_H}{\rho_e}, \tag{4}$$

where e_c is the electron charge.

C. Error analysis

The uncertainty ΔF of a property F was calculated using the relation

$$\Delta F(x_1, x_2, \ldots) = \left[\sum_{i=1}^{n} \left(\frac{\partial F}{\partial x} \Delta x_i \right)^2 \right]^{1/2}, \tag{5}$$

where

$$\begin{aligned}
F(x_1, x_2, \ldots) &= \alpha_S(\Delta\varphi, T_h, T_c) \\
&= \rho_e(R_e, w, L_{te}, L) \\
&= \alpha_S^2/\rho_e(\alpha_S, \rho_e) \\
&= R_H(R_e, L_{te}) \\
&= n_c(R_H) \\
&= \mu(R_H, \rho_e). \tag{6}
\end{aligned}$$

The results are shown in Table I.

For α_S, which was obtained from two samples of the same film that were mounted side by side in the probe (Fig. 2), variations in repeatability were also taken into account. The Seebeck coefficient was measured on each sample after heating and waiting 20–30 min for steady state, and also after cooling. So, data were collected twice for each sample, totaling four measurements for each film. The difference between the maximum and minimum value of these four measurements was calculated in terms of a fraction of the averaged α_S. This was compared with the result from Eq. (5), and the larger value was taken as the uncertainty in α_S.

The accuracy of the ρ_e was limited by the uncertainties in A_t and L, while for R_H, the limit was found by drifts in R_e (or $\Delta\varphi$). Measurements of R_H were not completed when drifts were above 10%, which limited the data collection to only few points in the Bi–Te system. The electrical contacts, which were made with silver paint, were suspected to be
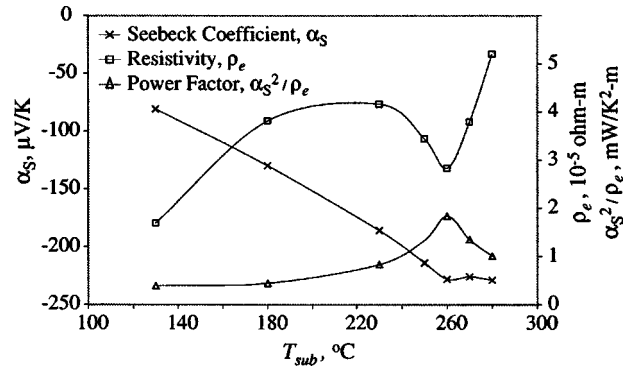

FIG. 3. Effect of T_{sub} on the TE properties, where the Te concentration (averaged over ten points for each sample) varied from 59.7% to 60.9%. (The lines are used only to guide the eye.)

causing this problem. Metallic (Cu or Au) contacts can be patterned prior to or after the TE film deposition, for future measurements.

IV. OPTIMUM POWER FACTOR IN THE BISMUTH-TELLURIUM SYSTEM

A. Effect of substrate temperature on thermoelectric properties of Bi–Te films

One-micron-thick Bi–Te films with Te concentration around 60% were deposited on a glass substrate at temperatures varying from 130 to 280 °C. In Fig. 3, the measured TE properties are shown for the various films. The Seebeck coefficient is negative indicating that the films are n-type, and its absolute value increases with T_{sub} up to 260 °C, where it reaches a plateau. Also, at this temperature ρ_e has a minimum, and the power factor, α_S^2/ρ_e, has its optimum value. At higher temperatures, because Te can reevaporate from the substrate leaving point defects (e.g., a vacancy or an antisite defect) in the crystal structure, ρ_e, which is sensitive to these defects, increases sharply.

The lower values of α_S at $T_{sub} < 260$ °C can be an indication that other Bi–Te phases coexist with Bi_2Te_3. For pure Bi (although it is unlikely to find unreacted Bi in the films), α_S is -50 and -100 μV/K for directions parallel and perpendicular to the trigonal axis, respectively.[12] The film composition was measured at ten distinct locations on the sample, as previously mentioned, and for an analytical volume of about 1–2 μm^3, the at. % Te varied from 59.3 to 60.1, for the film deposited at 130 °C. Although these values might indicate that the compound is Bi_2Te_3, they could be an average of various phases, since the area analyzed with the microprobe covers hundreds of grains for the low-temperature film, as can be inferred from Fig. 4(a). The surface SEM micrograph of the film coevaporated at 260 °C, with at. % Te of 60, is shown in Fig. 4(b), where grains as large as 0.5 μm are evident. The dashed lines at the cross-sectional view are highlighting the grain boundaries. Voids are observed in the cross section of the film deposited at 130 °C [Fig. 4(a)], and the grain boundaries, although appearing to be closer to each other than in the higher T_{sub} films, are not well defined.
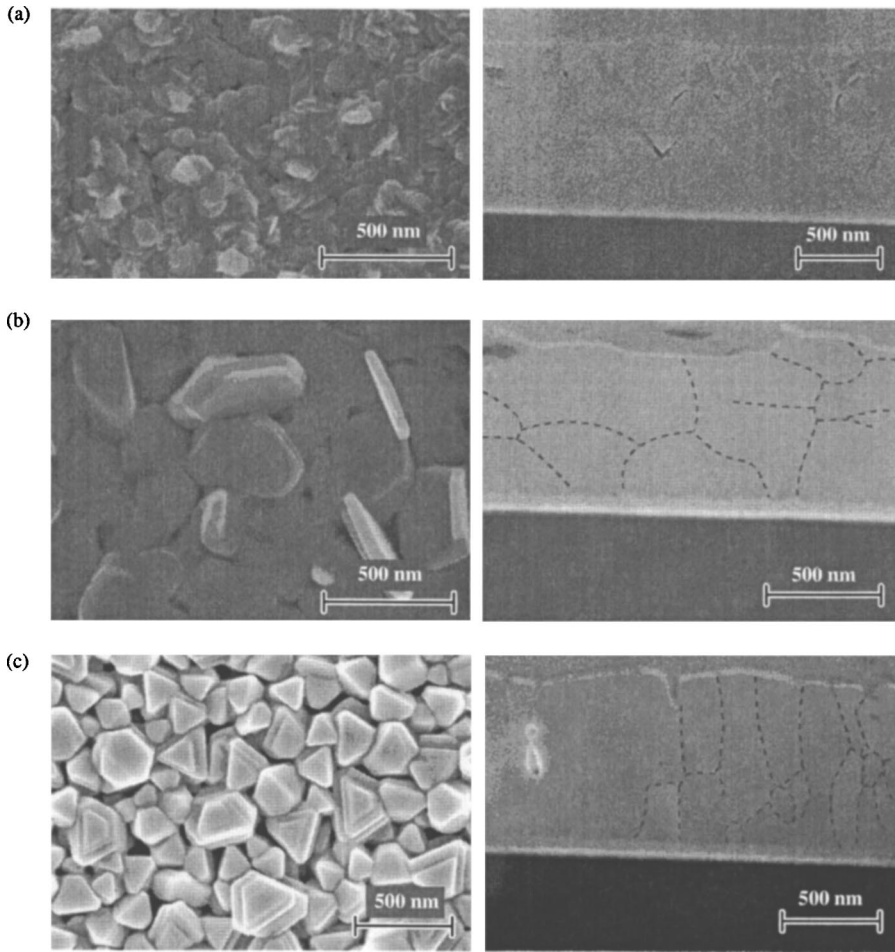
(a)

(b)

(c)

FIG. 4. SEM micrograph showing the top and cross section of the coevaporated Bi_2Te_3 films deposited at (a) 130 and (b) 260 °C, both with at. %Te of 60, and (c) 260 °C with at. %Te of 54. The bar on the bottom right of each SEM micrograph corresponds to a length of 500 nm (on scale). In (b) and (c), the dashed lines at the cross-section views are highlighting grain boundaries.

In Table II, R_H, n_c, and μ are presented for films deposited at T_{sub} of 250, 260, and 280 °C. Among the films with 60% of Te, the one deposited at 260 °C, which has the highest power factor, also has the highest mobility (presumably because it is very close to a true Bi_2Te_3 stoichiometry and thus has a minimal number of defects). High mobilities are expected for crystal structures with large grain sizes since they tend to reduce boundary scattering of carriers.

The diffraction patterns of powdered Bi_2Te_3 single crystal, and of the Bi–Te films, are shown in Figs. 5(a)–5(c). The position of the peaks agrees with the associated entries in the Powder-Diffraction File for Bi_2Te_3,[13] and the corresponding reflection planes (hkl) are labeled.

The three highest relative intensities, I/I_o, reported in Ref. 13, correspond to the planes (015) ($I/I_o=100$), (1.0.10) ($I/I_o=25$), and (110) ($I/I_o=25$). For other peaks $I/I_o \leqslant 8$.

TABLE II. Measured Hall coefficient R_H, carrier concentration n_c, and mobility μ of Bi–Te films, at room temperature.

T_{sub}(°C)	at. % Te	$R_H(10^{-6}$ m³/C)	$n_c(10^{25}$ m⁻³)	$\mu(10^{-4}$ m²/V s)
250	60	−0.063	9.9	2
260	60	−0.355	1.8	125
280	60	−0.270	2.3	52
260	59.7	−0.017	37	2.9
260	57.6	−0.006	96	9.6
260	54.0	−0.003	196	10.6

Note in Fig. 5 that these three strongest peaks are seen in the spectra of the reference-powdered Bi_2Te_3 (a) and of the films deposited at 130 °C (b) (the relative intensities are different). These reflection planes indicate no preferential crystallite orientation of samples (a) and (b), which was expected for (a), since the powdered grains are randomly oriented. We tried to match the x-ray spectra of other possible phases (apart for Bi_2Te_3) within the Bi–Te system but found no convincing match.

The intensities of the diffraction peaks corresponding to (00l) planes (c-axis preferentially oriented, perpendicular to the substrate surface) become significant at T_{sub} of 230 °C (not shown here), and increase at higher temperatures. They are dominant in the film deposited at 260 °C [Fig. 5(c), peaks corresponding to (006) and (0.0.15) planes], which had the highest power factor (Fig. 3).

In Fig. 6, the diffraction patterns of the Bi–Te films deposited at 130 and 260 °C are enlarged to show the effect of T_{sub} on the linewidth of the peaks. The smaller linewidths observed in Fig. 6(b), when compared with (a), indicate an increase in the grain size with the increase of T_{sub}, and suggest higher crystalline quality. This result is in agreement with Figs. 4(a) and 4(b). Such physical characteristic of the films can also be affecting the TE properties (as previously discussed for mobility).
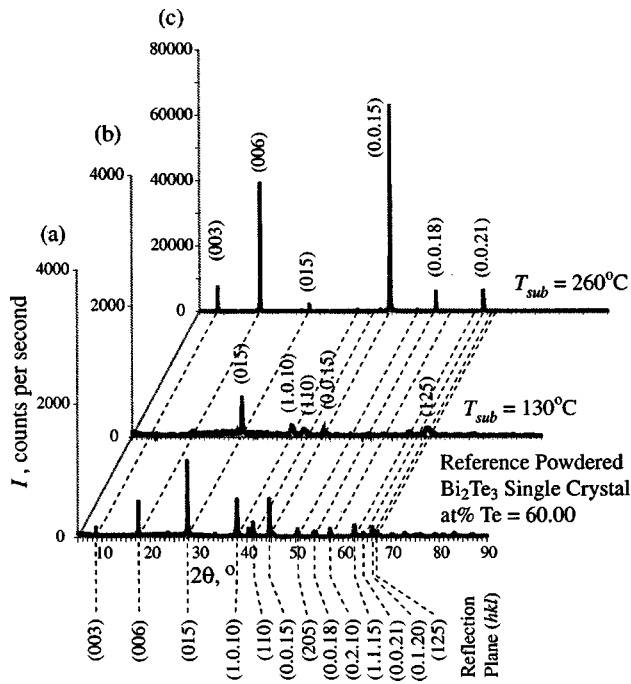
FIG. 5. X-ray diffraction patterns of reference-powdered Bi_2Te_3 single crystal (a), and coevaporated Bi_2Te_3 films (at. % Te ~ 60) deposited on a glass substrate at 130 °C (b), and at 260 °C (c). The positions (diffraction angle 2θ) of the measured peaks agree with the Powder-Diffraction File (see Ref. 13).

B. Effect of film composition on thermoelectric properties of Bi–Te films

Bi–Te films were deposited on glass substrates at various stoichiometries for T_{sub} of 260 and 130 °C. The effect of film composition on the TE properties can be seen, at these temperatures, in Figs. 7(a) and 7(b). The optimum power factors, given in Table III for both T_{sub}, were found for at. % Te of approximately 60. Note that in Fig. 7(a), films with at. % Te > 60 could not be obtained due to the reevaporation of Te from the substrate.

In the XRD patterns (not presented here), no effect of composition on the predominant orientation of the films
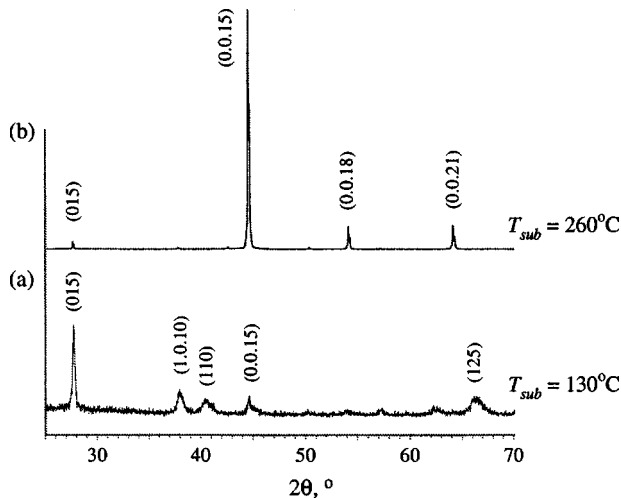

FIG. 6. X-ray diffraction patterns of Bi–Te films deposited at 130 (a) and 260 °C (b), showing the effect of T_{sub} on the linewidths.
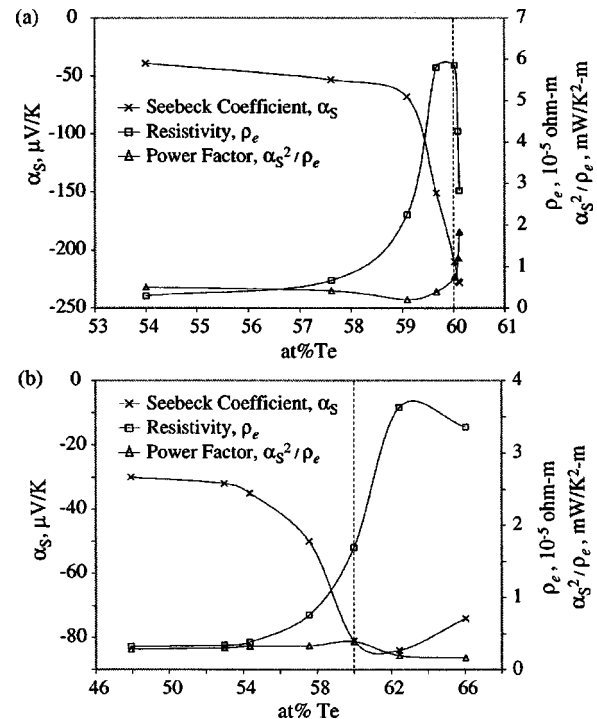

FIG. 7. Effect of Te composition on the TE properties of Bi–Te films deposited on a glass substrate at (a) 260 and (b) 130 °C. (The lines are used only to guide the eye.)

(c-axis for films deposited at T_{sub} of 260 °C, and random for films deposited at T_{sub} of 130 °C) was observed.

Hall coefficients for films deposited at 260 °C, given in Table II, indicate a reduction of the carrier concentration n_c with the increase in the Te content. The mobility μ has a maximum at at. % Te of 60. Note that, although μ is about ten times lower for the film with at. % Te of 54, its resistivity ρ_e is also lower compared with the film with 60% of Te, as shown in Fig. 7(a), due to its higher n_c (ρ_e is inversely proportional to the product between μ and n_c).

The top surface of the films with at. % Te of 60 and 54 (both deposited at 260 °C) is shown in Figs. 4(b) and 4(c), respectively. The film with a larger grain size is richer in Te and has higher carrier mobility. The cross sections are also presented, where this difference in the grain size is clearly indicated by the grain boundaries highlighted with dashed lines.

C. Effect of substrate material and crystal structure on thermoelectric properties of Bi–Te films

Bi–Te films were coevaporated on glass (type-II soda lime), Al_2O_3 (0001), MgO (100), mica, and Pt substrates at T_{sub} of 260 °C. The effect of film composition on the TE properties is shown in Figs. 8(a)–8(c) for all substrates, with

TABLE III. Measured optimum TE properties of coevaporated Bi–Te films deposited at 260 and 130 °C.

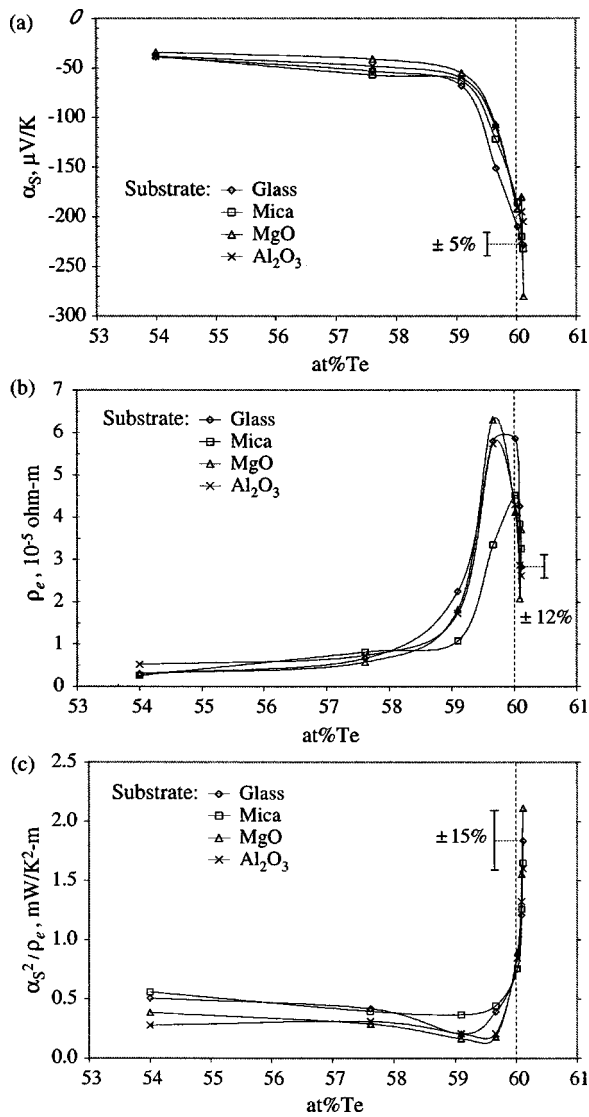| T_{sub}(°C)	ρ_e($\mu\Omega$ m)	α_S(μV/K)	α_S^2/ρ_e(mW/K^2 m)	at. % Te	L_{te}(μm)
260	28.3	−228	1.84	60.11	1.0
130	16.9	−81	0.39	59.99	1.3

FIG. 8. Thermoelectric properties of Bi–Te films deposited at 260 °C on glass, mica, MgO, and Al$_2$O$_3$ substrates. (The lines are used only to guide the eye.)

TABLE IV. Reflection planes of Bi–Te films deposited on various substrates at T_{sub} of 260 °C and for at. % Te around 60.

Substrate	(hkl)
Glass	$(00l)+(015)$
Pt	$(00l)+(015)$
Mica	$(00l)+(015)+(0.2.10)$
Al$_2$O$_3$	$(00l)+(015)+(205)$
MgO	$(00l)+(015)+(205)+(1.1.15)$

entation for the Bi$_2$Te$_3$ crystal structures grown on glass and Pt, while crystals grown on MgO are more randomly oriented.

The XRD patterns of the Bi–Te film deposited on glass and Pt (at 260 °C and with at. % Te of 60.11) are shown in Figs. 9(a) and 9(b), respectively. In (c) is the spectra of the Pt substrate, which should be subtracted from (b), in order to properly compare (a) and (b). Note that the same $(00l)$ peaks are detected in both films, and the relative intensities of most of them are similar.

V. OPTIMUM POWER FACTOR IN THE ANTIMONY-TELLURIUM SYSTEM

A. Effect of substrate temperature on thermoelectric properties of Sb–Te films

The measured α_S and ρ_e, and the calculated α_S^2/ρ_e of Sb–Te films deposited on glass, are shown in Fig. 10 as a function of T_{sub}. The tellurium concentration varies from 60.0% to 61.1% among the films, which are approximately 1 μm thick. The Seebeck coefficient is positive indicating that the films are p-type. Note that the maximum α_S and the

the exception of Pt (substrates with high electrical resistivity are required to allow for reliable measurements of TE properties).

At a given at. % Te, the variation of film composition among the substrates was found to be within ±0.5%. Although the highest power factor was obtained for a film grown on MgO (at. % Te of 60.1), this is not the case for other Te compositions. Therefore, to within an uncertainty of 15%, no significant effect of the substrate (material and crystal structure) on the TE film properties is evident. This is an indication that films grown on Pt are likely to present similar performance as the ones reported here.

In the XRD patterns, the position of the peaks agrees with the associated entries in the Powder-Diffraction File for Bi$_2$Te$_3$,[13] for all substrates (including Pt), and no significant effect of at. % Te on the crystal structure of the films was observed. The reflection planes verified in the films with at. % Te around 60 are listed in Table IV, where l is equal to 3, 6, 15, 18, and 21. The peaks from the $(00l)$ planes presented higher intensities. The c-axis is the predominant ori-
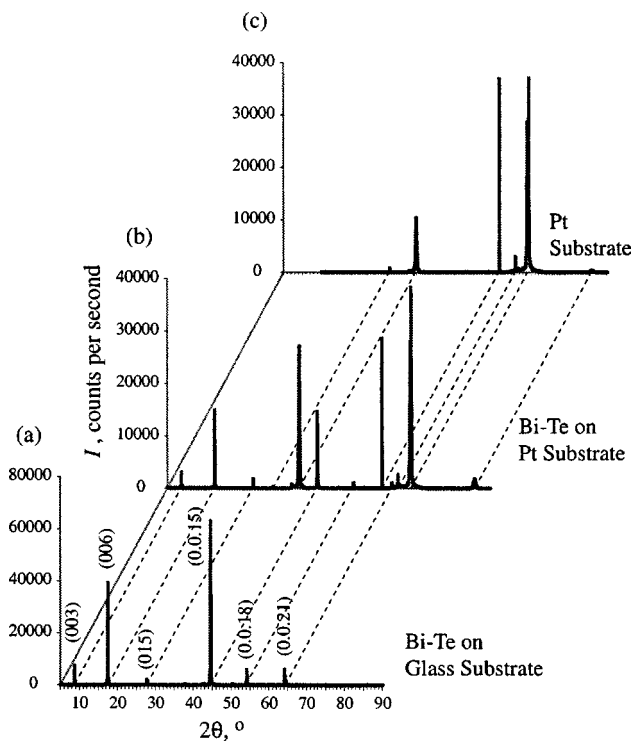

FIG. 9. X-ray diffraction patterns of a Bi–Te film deposited on glass (a) and Pt (b) (at 260 °C and with at. % Te of 60.11) and of the Pt substrate (c).
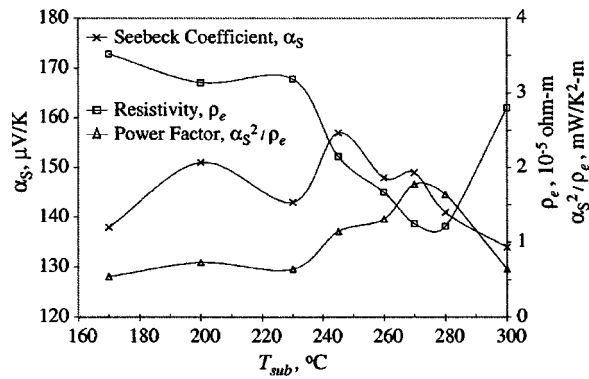
FIG. 10. Effect of T_{sub} on the TE properties, where the Te concentration (averaged over ten points for each sample) varied from 60.0% to 61.1%. (The lines are used only to guide the eye.)

minimum ρ_e do not occur at the same temperature, as observed for the Bi–Te system in Fig. 3. The optimum power factor is found at T_{sub} around 270 °C.

For $T_{sub} < 270$ °C, the difference between the maximum and minimum α_S is about 15% of their average (Fig. 10), while in the Bi–Te system this value increases to 80% (Fig. 3). This lower sensitivity of α_S to T_{sub} in the Sb–Te compounds can be due to the higher background carrier density of this system compared with Bi–Te. Because the maximum of the solids curve in the Sb–Te phase diagram is shifted towards the side of Sb, crystals of Sb_2Te_3 prepared from stoichiometric melts are always p-type conductors and contain high concentrations of holes, on the order of 10^{26} m^{-3}

(almost one order of magnitude higher than Bi_2Te_3, which is presented in Table II for at. % Te of 60).[14,15] Moreover, because the formation energy for antisite defects (Sb on the Te sublattice) is low, Sb_2Te_3 crystals also contain a high density of such defects.

The lower values of ρ_e shown in Fig. 10, when compared with the results from Fig. 3, can also be attributed to the higher background carrier density (or higher n_c) of Sb–Te films. As found from Eq. (4), ρ_e is inversely proportional to n_c.

The surface SEM micrographs of the film coevaporated at 170 and 270 °C are shown in Figs. 11(a) and 11(b), respectively, with magnifications of $60\,000\times$ and $15\,000\times$ (where the latter indicates homogeneity in the grain structure). The grain size increases with T_{sub}, and an increase in carrier mobility μ is expected, as discussed in Sec. IV A. This is in agreement with the decrease of ρ_e as T_{sub} increases, observed in Fig. 10, since ρ_e is inversely proportional to μ [Eq. (4)]. At high T_{sub}, reevaporation of Te from the substrate occurs (which creates point defects in the crystal structure), causing the increase of ρ_e.

The diffraction patterns of powdered Sb_2Te_3 single crystal, and the Sb–Te films deposited at T_{sub} of 170 and 270 °C are shown in Figs. 12(a)–12(c). The position of the peaks agrees with the associated entries in the Powder-Diffraction File for Sb_2Te_3,[13] and the corresponding reflection planes (hkl) are labeled.

The three highest relative intensities, I/I_o, reported in Ref. 13, correspond to the planes (015) ($I/I_o = 100$), (1.0.10)
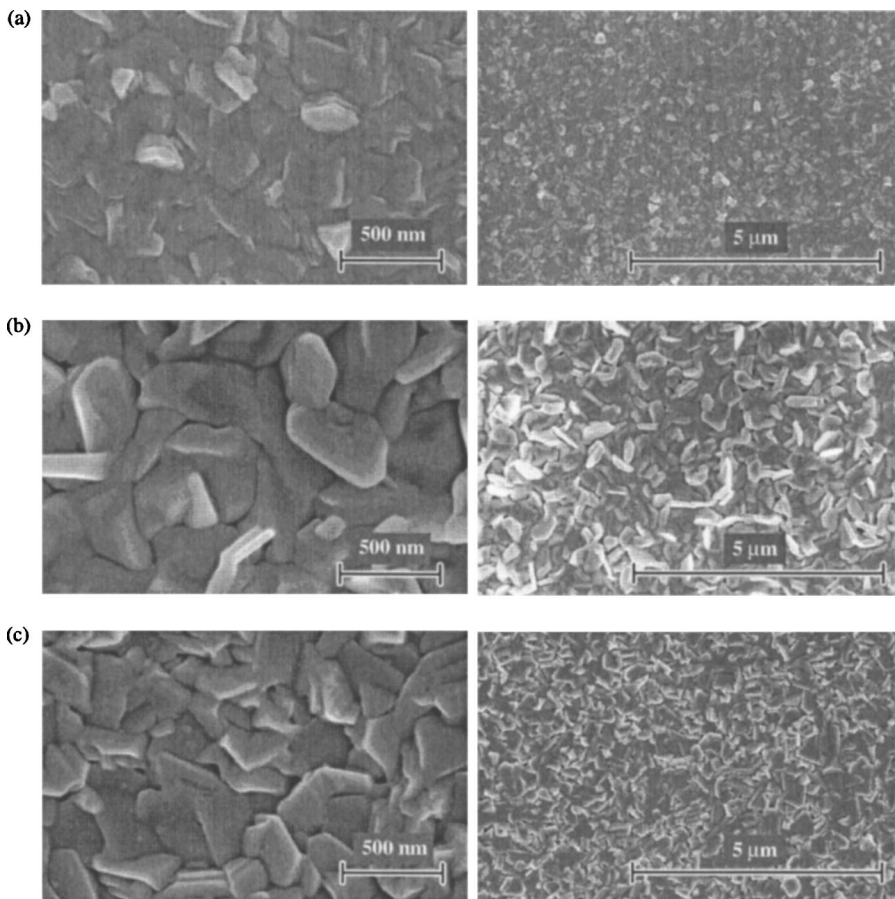

FIG. 11. SEM micrograph showing the top views of the coevaporated Sb–Te films deposited at (a) 170 and (b) 270 °C, both with at. % Te around 60, and (c) 270 °C with at. % Te about 50. Each micrograph on the right shows a larger area of the same film, indicating uniformity of the grain structure.

FIG. 12. X-ray diffraction patterns of reference-powdered Sb_2Te_3 single crystal (a), and coevaporated Sb_2Te_3 films (at. % Te $\sim$ 60) deposited on a glass substrate at 170 (b) and 270 °C (c). The positions (diffraction angle 2θ) of the measured peaks agree with the Powder-Diffraction File (see Ref. 13).

FIG. 13. X-ray diffraction patterns of Sb–Te films deposited at 170 (a) and 270 °C (b), showing the effect of T_{sub} on the linewidths.

films deposited on a glass substrate at 270 and 170 °C, respectively. The effect on the TE properties can be seen in Fig. 14. The optimum power factors are given in Table V.

At T_{sub} of 270 °C, because the measured results do not follow a smooth curve, each property is plotted separately

$(I/I_o = 35)$, and (110) $(I/I_o = 25)$. For other peaks $I/I_o \lesssim 10$. Note that in Fig. 12, these three strongest peaks are seen in the spectra of the reference-powdered Sb_2Te_3 (a) and the two highest peaks are dominant in the film deposited at 170 °C (b) (the relative intensities are different). These reflection planes indicate no preferential crystallite orientation of samples (a) and (b), which was expected for (a), since the powdered grains are randomly oriented. No convincing match with the x-ray spectra of other possible phases (apart from Sb_2Te_3) within the Sb–Te system was found.

In the XRD spectra for the film deposited at 270 °C [Fig. 12(c)], and at higher substrate temperatures (not shown here), the intensity of the diffraction peaks that correspond to (00*l*) planes increased relatively to the other peaks identified in the films deposited at lower T_{sub}. It is evident that as T_{sub} increases, the Sb–Te crystal structures become more *c*-axis oriented.

In Fig. 13, the XRD spectra of the films deposited at 170 and 270 °C are enlarged (for 2θ varying from 37° to 47°) in order to show the difference in the linewidths between the peaks of the two films. As T_{sub} increases, the linewidths decrease (peaks are sharper), suggesting higher crystalline quality. This result is in agreement with the increase in the grain size shown in Fig. 11, as T_{sub} increases.

B. Effect of film composition on thermoelectric properties of Sb–Te films

The composition of the Sb–Te films was varied from approximately 50 to 62 at. % Te, and 50 to 74 at. % Te, for

FIG. 14. Effect of Te composition on the TE properties of Sb–Te films deposited on a glass substrate at (a) to (c) 270 and (d) 170 °C. (The lines are used only to guide the eye.)

TABLE V. Measured optimum TE properties of coevaporated Sb–Te films deposited at 270 and 170 °C.

T_{sub}(°C)	$\rho_e(\mu\Omega$ m)	$\alpha_S(\mu$V/K)	α_S^2/ρ_e(mW/K^2 m)	at. % Te	$L_{te}(\mu$m)
270	12.5	149	1.78	60.53	1.1
170	25.5	126	0.62	58.85	1.0

with error bars [Figs. 14(a)–14(c)], where an approximate best-fit line is drawn as a guide to the eye. The optimum power factor is found for a film slightly rich in Te. The peak in Fig. 14(c) is located on the right side of the vertical dashed line (which marks the Sb$_2$Te$_3$ stoichiometry), where the resistivity has a minimum [Fig. 14(b)]. The peak found for ρ_e at at. % Te of 59.5 might be due to a defect structure forming around that composition.

The top surfaces of the films with at. % Te of 60 and 50 (both deposited at 270 °C) are shown in Figs. 11(b) and 11(c), respectively. The one richer in Te has a larger grain size, again indicating that its mobility is likely to be higher. In contrast to the Bi–Te system, where ρ_e at 60% Te was about six times larger than that at 54% [Fig. 7(a)], the Sb–Te system does not show significant differences in ρ_e at these compositions [Fig. 14(b)]. The difference in carrier concentration should not be as pronounced as the one measured for Bi–Te (Table II), due to the higher background carrier density of the Sb–Te films near stoichiometry.

The power factor of the films deposited at 170 °C [Fig. 14(d)] slightly increases around 60% Te, and then reaches a plateau. No effect of composition on the crystal orientation of these films is found (they are polycrystalline).

For films deposited at 270 °C, the XRD patterns (not shown here) indicate that at at. % Te about 60 and above it, the intensities of the peaks corresponding to (00*l*) planes increase significantly [the highest corresponding to (0.0.15)]. Below 60% Te, films are polycrystalline [with the highest peak corresponding to plane (015)].

C. Effect of substrate material and crystal structure on thermoelectric properties of Sb–Te films

Additional substrates, such as Pt, Al$_2$O$_3$, MgO, and mica (the same type used in the Bi–Te system analysis), were included, together with glass, in each of the coevaporations of Sb–Te, at T_{sub} of 270 °C, discussed in the previous sections.

All films deposited on MgO and mica, and most of the films on Al$_2$O$_3$, had a rather poor quality. The films appeared transparent on these substrates and no electrical continuity was found in them. The exceptions were the films deposited on Al$_2$O$_3$ at 270 °C, with at. % Te of 58.5, 58.9, and 59.3. However, the thicknesses of these three films on Al$_2$O$_3$ were about 20% smaller than the values measured for the same films grown on glass (around 1 μm). It is evident that there are problems with Sb–Te sticking to these substrates. The crystal structure of Sb$_2$Te$_3$ is very similar to Bi$_2$Te$_3$ (rhombohedral with five atoms in the primitive unit cell),[16] and therefore, we would expect no significant effect of the substrate on the TE properties of Sb–Te films, as verified for the Bi–Te system.

X-ray diffraction analyses show that on Al$_2$O$_3$, the Sb–Te crystal structures were strongly *c*-axis oriented, while on Pt, no preferential orientation was detected. Because it was not possible to compare the measured TE properties of the films deposited on glass with the other substrates, and also, because the films deposited on Pt did not have the *c*-preferential orientation verified for the films with optimum power factor deposit on glass, the question remains if the films deposited on Pt will have the same TE properties as the films deposited on glass.

VI. CONCLUSIONS

For Bi–Te, the highest power factors were obtained at at. % Te around 60, for films deposited at T_{sub} of 260 °C (2.11 and 1.84 mW/K^2 m for deposition on MgO and glass, respectively). Comparing this result with the ones given in Fig. 1, it is verified that the optimum *n*-type film reported by Zou *et al.*,[3] which was also deposited by coevaporation at 260 °C, presented the same value of α_S listed in Table III. However, α_S^2/ρ_e is about two times lower than in Ref. 3, due to the differences in ρ_e. The *n*-type film reported by Böttner[6] yielded a lower value of the power factor.

The crystalline quality of the Bi–Te films reported here, deduced from the linewidths of the XRD patterns and from the SEM micrographs, was affected by T_{sub}. No effect of composition on crystal orientation was seen. Based on the limited number of tests performed, no significant effect of the substrate material and crystal structure on the TE properties was observed, within an uncertainty of ±15%. This is an indication that Bi–Te films deposited on Pt are likely to have the same performance as the films deposited on glass, Al$_2$O$_3$, MgO, or mica. The XRD pattern indicates that Bi$_2$Te$_3$ forms on Pt (at T_{sub} of 260 °C), which supports its use in the connector of the micro-TE cooler, as the metal that interfaces with the TE elements.[11]

The higher carrier concentration of Sb–Te films did affect the TE properties. The Seebeck coefficient was found to be less sensitive to T_{sub} and the electrical resistivities in general were lower, compared with the Bi–Te system. The highest power factor (1.78 mW/K^2 m) was obtained for a film deposited at 270 °C, with at. % Te of 60.5. This result can be compared with the ones reported in Fig. 1. In Ref. 3, the best *p*-type film was deposited at 230 °C and had α_S^2/ρ_e of 2.8 mW/K^2 m. This difference in performance is mostly due to α_S, since the resistivities are comparable, as can be seen in Table V. The *p*-type ternary compound fabricated by cosputtering,[6] which was annealed after deposition, yielded significantly higher α_S, but also had a higher ρ_e than the other optimum *p*-type Sb–Te films.

The SEM micrographs and the linewidths in the XRD patterns reported here for Sb–Te films indicate an increase in the crystalline quality with the increase of T_{sub}. Films deposited at 270 °C become preferentially *c*-axis oriented for at. % Te above 60, while no effect of composition was found for films deposited at 170 °C. Thermoelectric properties were measured only for films on a glass substrate due to the poor quality of the Sb–Te films deposited on Al$_2$O$_3$, MgO, and mica. The films grown on Pt were analyzed by XRD and

showed no preferential orientation, while *c* orientation was found for optimum films grown on glass. This is an indication that the TE properties of films grown on Pt substrate might also differ from those grown on glass. Due to the limited data, no conclusion can be drawn on the effect of substrate (material and crystal structure) on the TE properties of Sb–Te films. A more extensive investigation is needed.

ACKNOWLEDGMENTS

[1] D. A. Wright, Nature (London) **181**, 834 (1958).

[2] R. Venkatasubramanian, E. Siivola, T. Colpitts, and B. O'Quinn, Nature (London) **413**, 597 (2001).

[3] H. Zou, D. M. Rowe, and S. G. K. Williams, Thin Solid Films **408**, 270 (2002).

[4] J. R. Lim, G. J. Snyder, C.-K. Huang, J. A. Herman, M. A. Ryan, and J.-P. Fleurial, Thermoelectric Microdevice Fabrication Process and Evaluation at the Jet Propulsion Laboratory (JPL), *Proceedings of the 21st International Conference on Thermoelectrics*, Long Beach, California, (2002) (unpublished), pp. 535–539.

[5] H. Böttner *et al.*, J. Microelectromech. Syst. **13**, 414 (2004).

[6] H. Böttner (private communication).

[7] T. C. Harman, P. J. Taylor, M. P. Walsh, and B. E. Laforge, Science **297**, 2229 (2002).

[8] A. Majumdar, Science **303**, 777 (2004).

[9] D. Vashaee and A. Shakouri, Phys. Rev. Lett. **92**, 106103 (2004).

[10] L. W. da Silva and M. Kaviany, Int. J. Heat Mass Transfer **47**, 2417 (2004).

[11] L. W. da Silva and M. Kaviany, J. Microelectromech. Syst. (accepted for publication).

[12] C. F. Gallo, B. S. Chandrasekhar, and P. H. Sutter, J. Appl. Phys. **34**, 144 (1963).

[13] Joint Committee on Powder Diffraction Standards (JCPDS), Powder Diffraction File, Card Nos. 15-874 and 15-863, Pennsylvania (1983).

[14] H. Scherrer and S. Scherrer, *CRC Handbook of Thermoelectrics*, edited by D. M. Rowe (CRC, Boca Raton, FL, 1995), p. 211.

[15] V. A. Kulbachinskii *et al.*, Phys. Rev. B **52**, 10915 (1995).

[16] M. Stordeur, *CRC Handbook of Thermoelectrics*, edited by D. M. Rowe (CRC, Boca Raton, FL, 1995), p. 239.